PAPER • OPEN ACCESS

Refractive index measurement of hydrogen isotopologue mixture and applicability for homogeneity of hydrogen solid at cryogenic temperature in fusion fuel system

To cite this article: Jiaqi Zhang *et al* 2023 *Nucl. Fusion* **63** 076020

OPEN ACCESS
IOP Publishing | International Atomic Energy Agency
Nuclear Fusion
Nucl. Fusion **63** (2023) 076020 (9pp)
https://doi.org/10.1088/1741-4326/acd015

Refractive index measurement of hydrogen isotopologue mixture and applicability for homogeneity of hydrogen solid at cryogenic temperature in fusion fuel system

Jiaqi Zhang[1,*], Akifumi Iwamoto[2], Keisuke Shigemori[1], Masanori Hara[3] and Kohei Yamanoi[1]

[1] Institute of Laser Engineering, Osaka University, 2-6 Yamadaoka, Suita, Osaka 565-0871, Japan
[2] National Institute for Fusion Science, 322-6 Oroshi, Toki, Gifu 509-5292, Japan
[3] Faculty of Science, Academic Assembly, University of Toyama, 3190 Gofuku, Toyama 930-8555, Japan

E-mail: zhang-j@ile.osaka-u.ac.jp

Received 29 October 2022, revised 31 March 2023
Accepted for publication 25 April 2023
Published 6 June 2023

Abstract

Deuterium (D)-Tritium (T) nuclear fusion reaction has potential as an energy source in the future. In both magnetic confinement and inertial confinement fusion reactors, solid D–T will generally be supplied as fusion fuel. The efficiency of the nuclear fusion reaction depends on the quality of solid D–T fuel, which is related to the composition, homogeneity, helium-3 (^{3}He) content, and so on. However, there is no technique for *in-situ* examination of solid D–T fuel. In this study, we consider a simple and precise method for the characterization of solid hydrogen isotopologues at cryogenic temperature using refractive index measurement, and evaluate the distribution of hydrogen isotopologue composition and homogeneity. To evaluate without the effect of tritium decay, the homogeneity of the hydrogen (H_2)-deuterium (D_2) mixture is measured at first. By the *in-situ* refractive index measurement at cryogenic temperature, the homogeneity of solid H_2–D_2 mixture is roughly quantified. The phase diagram of the H_2–D_2 mixture shows a solid solution type. D_2-rich crystal first appears from the liquid phase as a primary crystal. The composition of D_2 in liquid phase ias homogeneous, whereas it reduces by obeying the liquidus line in the phase diagram with the crystallization. On the other hand, the composition of the H_2–D_2 mixture in solid phase is inhomogeneous because the mobility of H_2 and D_2 in solid phase was too slow to be homogeneous and solid. The compositions of H_2–D_2 mixture in liquid and solid phases could be evaluated by the *in-situ* refractive index measurement in time. Consequently, the refractive index measurement shows great potential as an inspection method of solid D–T fuel in fusion reactors.

* Author to whom any correspondence should be addressed.

Keywords: tritium, hydrogen isotopologues, fusion fuel, refractive index

(Some figures may appear in colour only in the online journal)

1. Introduction

As a fusion fuel, Deuterium (D)–Tritium (T) fuel has a large cross-section, considerable energy yield, and low ideal ignition temperature, making the D–T fusion reactor the most likely to first achieve self-reliant fusion [1]. To overcome the Coulomb barrier, the D–T fuel needs to be heated to a temperature at which it forms plasma. Magnetic Confinement Fusion (MCF) and Inertial Confinement Fusion (ICF) are two fundamental confinement technologies being investigated at present.

In ICF reactors, the solid fuel layer is contained in a tiny (few-millimeter diameter) hollow pellet, as shown in figure 1. Laser or heavy ion beams uniformly ablate the surface of the fuel pellet and produce the required compression and heating to implode the D–T fuel layer, leading to a fusion reaction. To accomplish the fusion reaction, the target pellet properties should be strictly controlled, including sphericity, surface roughness, thickness uniformity of multiple layers in the pellet, homogeneity of the solid D–T layer, etc. To date, formations of solid fuel layers have been studied for central and fast ignitions [2–6].

For MCF reactors, new D–T fuel should be continuously replenished into the reaction chamber as a puff of gas, stream of ions, or liquid or solid pellets. Fusion reaction is caused when magnetic and electric fields are used to heat and confine fuel as plasma. At present, pellet injectors are equipped on most tokamaks and stellarators because solid pellets can increase plasma density, and pellets can penetrate the plasma boundary before the molecules become ionized, adding fuel directly to the confined plasmas [7]. At cryogenic temperature, the pellet injectors typically generate numerous millimeter-sized solid D–T pellets with a cylindrical shape. Since the mass loss on the fuel surface occurs during transportation from the injector into the plasma [7], fuel homogeneity is critical to avoid distortion in the fuel component ratio.

Regardless, in MCF or ICF, high-quality solid fuel production is an important issue. Successful fusion reaction requires that the fuel meet many stringent specifications. During D–T fuel solidification, however, isotope effects and β-decay of T might affect the homogeneity and composition of the fuel, leading to a decrease in the fusion reaction efficiency. To maximize fusion reaction efficiency, D:T should be kept close to 50:50.

Thus, to realize the design and fabrication of high-quality solid D–T fuel and ensure the quality of the fuel entering the reactor, this study has demonstrated a method for characterizing the fuel homogeneity simply, accurately, and nondestructively using the optical measurement of the refractive index distribution of fuel. Firstly, for establishing an isotopologue distribution evaluation method in an environment without beta decay effects, we prepared the solid hydrogen (H_2)–deuterium (D_2) mixture to measure the refractive index. It can also be used as a preparatory experiment for solid D–T measurement.

2. Method

Solid D–T fuel would be characterized by its composition and homogeneity prior to use in fusion reactors. The refractive index measurement can simultaneously determine the hydrogen isotopologue composition and its homogeneity. In this study, the optical cell for the refractive index measurement, which has a wedge-shaped gas filling chamber, was used as shown in figure 2. The cell was put in the cryostat. The system detail was described in our previous literature [8]. In this section, the theory of the refractive index measurement is described at first, and the measurement procedure including the H_2–D_2 solidification is explained.

2.1. Temperature-dependent refractive index measurements of H_2 and D_2

When H_2–D_2 mixture is solidified by thermal conductivity, the H_2–D_2 mixture has a temperature gradient. Since the refractive index is a function of the density of hydrogen isotopologues, refractive index data for H_2 and D_2 in various conditions are indispensable. To calculate the refractive index of H_2 and D_2 at a given temperature, the empirical formula between density ρ and refractive index n, known as the Lorentz–Lorenz relation, was used:

$$\frac{M}{\rho}\cdot\frac{n^2-1}{n^2+2}=\frac{4\pi}{3}N_{\mathrm{A}}\alpha \tag{1}$$

where α is the molecular polarizability, M is the molecular mass, and N_{A} is the Avogadro constant. The specific refraction r_λ can be identified via the Lorentz–Lorenz relation

$$r_\lambda=\frac{1}{\rho}\cdot\frac{n^2-1}{n^2+2}. \tag{2}$$

The specific refraction is a function of wavelength. Cauchy's dispersion formula is an empirical expression giving an approximate relation,

$$r_\lambda=r_\infty+\frac{A}{\lambda^2}+\frac{B}{\lambda^4}, \tag{3}$$

where A and B are coefficients for λ in angstroms and r in $\mathrm{cm^3\ g^{-1}}$. The values of A and B depend on the medium. r_∞ is the specific refraction at $\lambda=\infty$. the r_∞ of hydrogen is related to molecular polarizability and is approximately independent of temperature and density over a wide range [9]. Based on

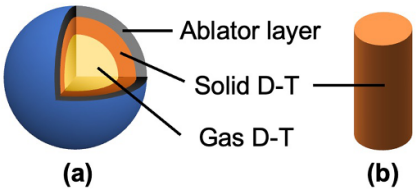

Figure 1. Schematic of solid fusion fuel. (*a*) ICF fuel pellet. (*b*) MCF fuel pellet.

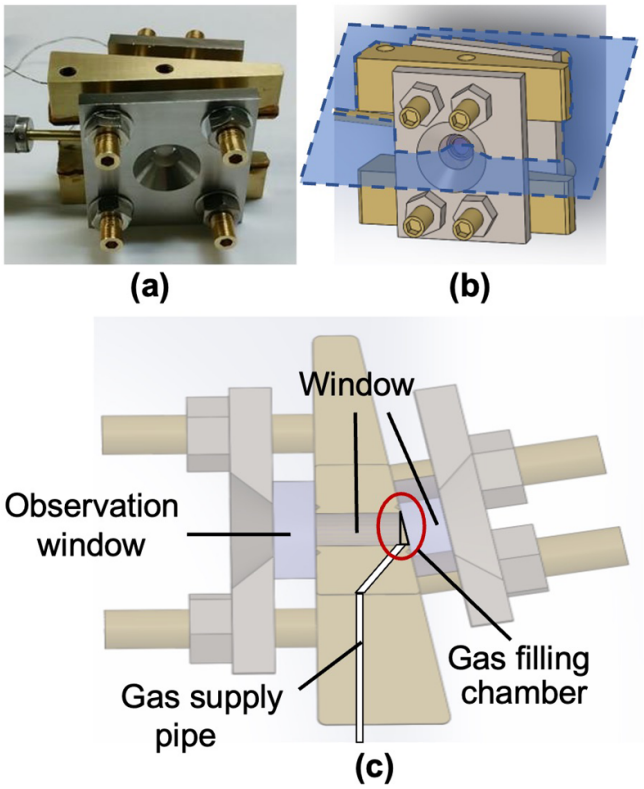

Figure 2. Optical cell for refractive index measurement. (*a*) Actual picture of the cell. (*b*) 3D model drawing of the cell. (*c*) Cross-section of the cell. Inner diameter of the filling chamber is 5 mm.

equations (2) and (3), the refractive index n, dependence of the density ρ, and wavelength of incident light (λ) are adequately represented by

$$n_i = \sqrt{\frac{3}{1-\rho\left(r_\infty + \frac{A}{\lambda^2} + \frac{B}{\lambda^4}\right)}} - 2. \tag{4}$$

The r_∞ coefficients A and B for H_2 and D_2 at STP conditions were reported by Childs and Diller [9]. These data were summarized in table 1.

For H_2 and D_2 in solid and liquid states, the density is strongly affected by temperature. The empirical formulas of density or molar volume as a function of temperature T (K) are as follows.

Liquid H_2 [10]:

$$\rho_m = 0.0134572 + 0.0092597 \times (32.984 - T)^{\left(\frac{1}{3}\right)} \tag{5}$$

Table 1. Parameters reported by Childs and Diller [9].

	A Å^{2}cm g^{-1}	B Å^{4}cm^3 g^{-1}	r_∞ cm^3 g^{-1}
H_2	0.7799569×10^6	0.495126×10^{12}	1.0050
D_2	0.3616378×10^6	0.432143×10^{12}	0.4983

Table 2. Standard deviations of refractive index.

	Standard deviations
Liquid H_2	0.000111
Solid H_2	0.000639
Liquid D_2	0.000643
Solid D_2	0.001389

where ρ_m (mole cm^{-3}) is mole density (ρ_m=ρ/M), M (g mol^{-1}) is molar mass, and ρ (g cm^{-3}) *is* density. The maximum deviation of the estimated mole density is 0.015% of the mole density.

Solid H_2 [11]:

$$V_m = 22.7121856 - 0.03716186 \times T + 0.00532275 \times T^2 \tag{6}$$

where V_m (cm^3 mol^{-1}) is mole volume ($V_m = M/\rho$), The estimated V_m should be in error by no more than 0.4%.

Liquid D_2 [12]:

$$V_m = 20.188 + 0.03587 \times T + 0.006565 \times T^2 \tag{7}$$

with V_m in cm^3 mole^{-1}. The standard deviation from this equation is 0.01 cm^3 mole^{-1} (or 0.04% of V_m).

Solid D_2 [13]:

$$\rho = 0.20459 - 0.000026337 \times T^2 \tag{8}$$

with ρ in g cm^{-3}. The standard deviation of the estimated density is 0.00156.

In this experiment, the wavelength is a fixed value ($\lambda = 543$ nm). Thus, we can calculate the refractive index for a given temperature using equations (4)–(8). The standard deviation of the refractive index can be calculated by the propagation of uncertainty. The standard deviations of the refractive index are shown in table 2.

However, there are few reports about the refractive index of solid H_2, liquid D_2, and solid D_2. There is not enough valid data to support the reliability of the empirical formula. The estimated values of solid D_2 in particular have considerable standard deviations. To improve the accuracy of the equation, the temperature dependence of the refractive index of H_2 and D_2 in the liquid and solid phases were measured by the same method as previous research [8].

2.2. *Refractive index distribution measurements of H_2–D_2*

In this experiment, H_2–D_2 mixture was used instead of D_2–T_2 mixture. Our previous experiment measured the refractive

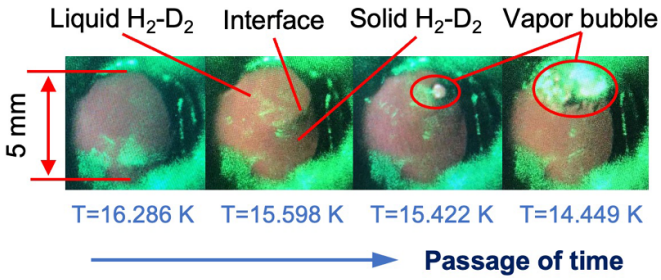

Figure 3. Solidification process of H_2–D_2 was observed in the observation window.

index of D_2–T_2, whereas H_2–D_2 mixture was used to observe the solidification behavior of hydrogen isotopologue without the effect of decay heat of tritium.

The H_2–D_2 mixture was made from the commercially available hydrogen gases where these purities were 99.999% for H_2 and 99.5% for D_2, and the gas composition was adjusted to be H_2:D_2 = 1:1. The solidification procedure is as follows.

(1) The temperature of the cell (see figure 2) was cooled down to 25.000 K; it was above the triple point of H_2 and D_2. Subsequently, gaseous H_2–D_2 was supplied to the cell.
(2) The bottom of the cell was gradually cooled, and the H_2–D_2 mixture was liquefied.
(3) The H_2–D_2 liquid became solid when the bottom of the cell was 16.074 K. A vapor bubble was observed at the top of the cell as shown in figure 3.
(4) The refractive index of liquid and solid H_2–D_2 was measured at optically flat points in the cell.

The refractive index of the H_2–D_2 mixture depends on the ratio of H_2 and D_2. If the refractive index is simultaneously measured at many points on the H_2–D_2 mixture, the distribution of H_2–D_2 would be known. Thus, the distribution of H_2 and D_2 can be determined by the refractive index distribution. A vertical refractive index distribution measurement system was constructed, as shown in figure 4. In this system, the point of the laser light as a primary incident light was dispersed into the line laser light by the cylindrical lens. The measurement procedure is as follows.

(1) The laser pattern of the incident laser as the reference position on the screen was determined by the laser passing through the prism cell in a vacuum.
(2) Subsequently, the H_2–D_2 mixture was loaded into the wedge-shaped optical cell. The H_2–D_2 mixture was liquefied and solidified in the cell as previously described.
(3) The line laser was refracted by passing the H_2–D_2 mixture in the cell. The position of the refracted laser on the screen was recorded. Figure 5 shows the typical photograph of laser patterns on the screen.
(4) The brightness of each pixel in the photograph was analyzed. To achieve the peak position of the laser pattern for the vertical direction, the brightness distribution of the laser pattern for the horizontal direction was fitted by the Gauss function.

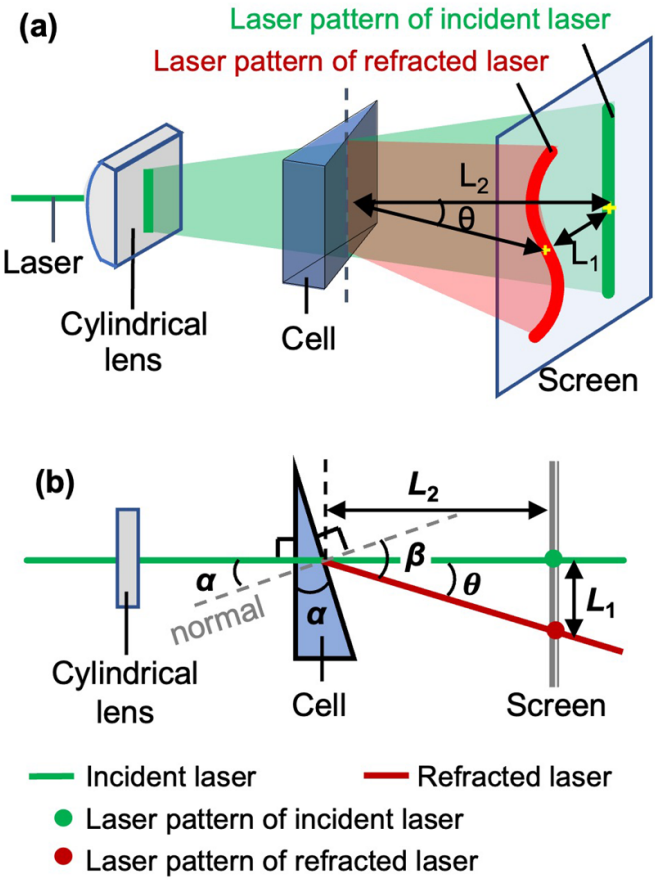

Figure 4. Calculation method of refractive index. (*a*) Schematic diagram of the vertical refractive index distribution measurement. (*b*) Cross-section of the vertical refractive index distribution measurement.

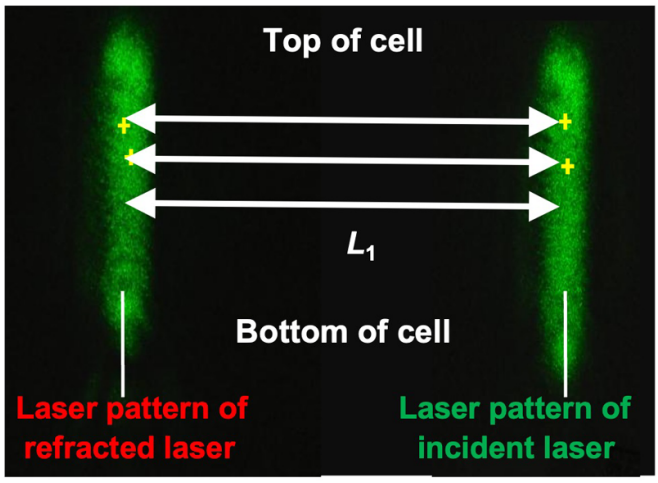

Figure 5. Photograph of laser patterns on the screen.

(5) The distance of the peak position between the incident and refracted lasers, L1 in figure 4(*b*), was calculated. The refracted angle by H_2–D_2, β (P) was calculated from

$$\beta(P) = \arctan\left[\frac{L_1}{L_2}\right] + \alpha. \tag{9}$$

The refractive index, $n_{HD}(P)$ is calculated by Snell's law,

$$n_{HD}(P)\cdot\sin\alpha = n_0\cdot\sin\beta(P). \tag{10}$$

The distribution of refractive index for the vertical direction was obtained.

(6) Using refractive index mixing rules can accurately predict the volume fractions of the mixture component. Various empirical and semi-empirical relations have been reported [14]. Among them, the Lorentz–Lorenz equation is approximately valid for solids as well as liquids and gases. The refractive indices of hydrogen [15] and deuterium [8] are calculated. The Lorentz–Lorenz mixing rule is represented as

$$\frac{{n_{HD}}^2-1}{{n_{HD}}^2+2} = \left(\frac{n_H^2-1}{n_H^2+2}\right)\phi_H + \left(\frac{n_D^2-1}{n_D^2+2}\right)\phi_D \tag{11}$$

where n_{HD}, n_H, and n_D are refractive indices of the H_2–D_2 mixture, H_2, and D_2, respectively. Φ_H and Φ_D are volume fractions of H_2 and D_2. For the convenience of calculation, the ratio of H and D was represented by the mole fraction of H_2 and the homogeneity of the H_2–D_2 mixture can be evaluated by the distribution of the H_2 mole fraction. The mole fraction of H_2, x_H, is calculated from

$$\phi_H = x_H v_H/(x_H v_H + x_D v_D) \tag{12}$$

$$x_H + x_D = 1 \tag{13}$$

where x_H is the mole fraction and v_H is the molar volume of H_2. x_D is the mole fraction and v_D is the molar volume of D_2.

3. Results and discussion

3.1. Temperature dependence of the refractive index of H_2 and D_2

The refractive indices of liquid and solid H_2 and D_2 were measured in the range of 13.752 K–15.000 K for H_2 and 13.579 K–21.984 K for D_2. The measurement uncertainty was calculated from the measurement error of the distance between the incident and refracted laser positions, L_1, by the propagation of uncertainty. The measurement uncertainties are 0.0000596 for solid H_2, 0.0000515 for liquid D_2, and 0.0000520 for solid D_2. Figure 6 shows the refractive indices of H_2 and D_2 as a function of the temperature. As the temperature decreased, the refractive index increased.

Although at cryogenic temperature, ortho-hydrogen tends to convert to para-hydrogen [16], and para-deuterium tends to convert to ortho-deuterium [17], the ortho–para conversion rate is slow without a catalyst or other facilitating mechanism. At 20.4 K, the temperature at 1 atmosphere pressure liquid normal-H_2 will be converted after several days and require weeks to approach equilibrium [18]. The ortho–para conversion rate of deuterium is slower than hydrogen [19]. The measurement time for solid H_2 was 1 h and solid D_2 was 2 h. In such a short period, the effect of ortho–para conversion was negligible [20]. Thus, in the study, the hydrogen is normal hydrogen (ortho–para ratio of 3:1), and the deuterium is normal deuterium (ortho–para ratio of 2:1).

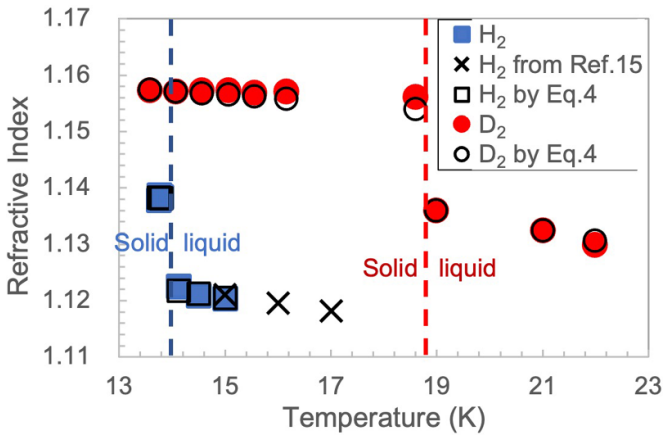

Figure 6. Refractive indices of H_2 and D_2 around their melting points.

The estimation values of refractive indices were calculated by analysis using equations (4)–(8). The measured values of refractive indices were compared with previous data and the estimation values. The refractive index obtained from liquid H_2 agrees with the values reported by Diller [15]. Other data also agreed with the estimation values. Namely, both the refractive index measurement and the analysis procedure were appropriate. However, the measured values of solid D_2 around the melting point were slightly higher than that estimated by equation (4), as seen in figure 6. The estimation of the refractive index of solid D_2 by equation (4) would be limited around the melting point. Thus, the relationship between the temperature and refractive index was fitted by the 2nd-order function. The function fitted to the refractive index of solid D_2 was

$$n = 1.148 + 0.0013349\times T - 0.000048494\times T^2. \tag{14}$$

The standard deviation was about 0.000193.

3.2. Homogeneity of solid H_2–D_2

Indeed, the isotopic exchange will lead the H_2–D_2 mixture to reach chemical equilibrium between H_2, D_2, and Hydrogen Deuteride (HD); but at ambient temperatures, this exchange reaction is slow (of many weeks) [21]. And the equilibrium constant for $H_2+D_2 \rightleftharpoons 2HD$ decreases with decreasing temperature [22]. The measurement time for solid H_2–D_2 mixture was 3 h. The HD generated by the isotopic exchange was negligible.

The refractive index vertical distribution of H_2–D_2 mixture at optically flat points in the cell was measured during solidification in the range of 13.415 K–16.498 K. Two typical results are shown in figure 7 for clarity. The blue curve shows the refractive index vertical distribution of the liquid H_2–D_2 mixture at 16.286 K. The red curve shows the refractive index vertical distribution at 15.598 K, the top part is liquid H_2–D_2,

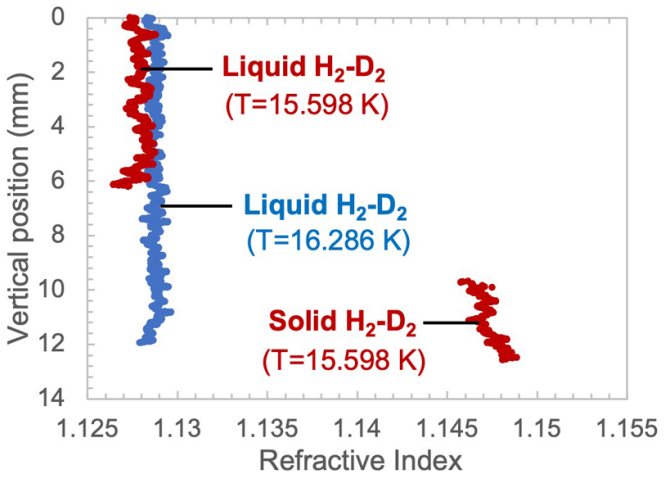

Figure 7. Refractive index vertical distribution of H_2–D_2. The temperature gradient is between the top and bottom of the cell. The cell was cooled down from the bottom of the cell.

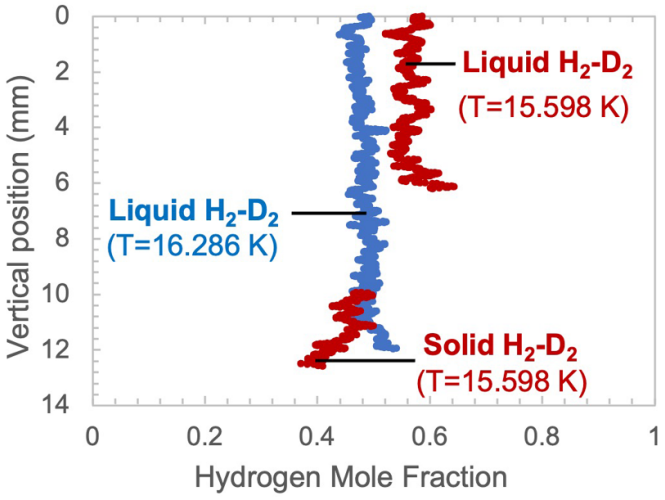

Figure 8. Mole fraction vertical distribution of H_2–D_2.

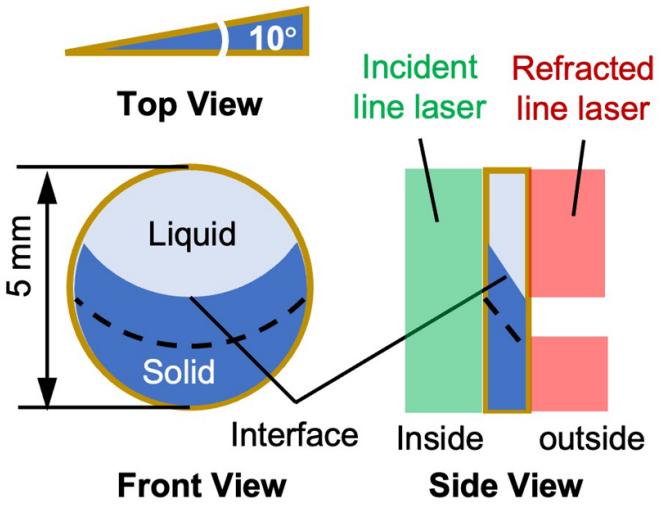

Figure 9. Three-view drawing of the filling chamber of cell at 15.598 K.

and the bottom part is solid H_2–D_2. The state of H_2–D_2 in the cell is shown in figure 3.

Since the temperature difference between the top and bottom of the cell was small, and the temperature dropped slowly, the temperature gradient can be regarded as an approximately uniform distribution in the vertical direction of the cell. Therefore, while measuring the refractive index, the temperature of this measurement point was also calculated, and the relationship between refractive index and temperature was obtained. The refractive index of H_2 and D_2, n_H *and* n_D, at a given temperature can be corrected by equation (4). Finally, the molar fraction distribution of H_2 was calculated using equations (11)–(13) as shown in figure 8. The statistical dispersions are 0.0334 for liquid H_2–D_2 and 0.0197 for solid H_2–D_2.

At 15.598 K, the mole fraction of H_2 in the solid phase gradually decreases approaching the bottom, meaning that the composition of H_2–D_2 in the primary crystal, which is the solid initially frozen, gave the higher D_2 composition rather than the original composition. This behavior can be explained by the H_2–D_2 phase diagram which is the solid solution type. This point will be described in detail later.

Additionally, at 16.286 K, the H_2 mole fraction of liquid H_2–D_2 was approximately homogeneous, which could be represented by the spatial average value, about 0.485. Theoretically, the H_2 and D_2 contents are conserved. At a different temperature, the spatial average of the mole fraction should be the same, but at 15.598 K, the spatial average of the H_2 mole fraction was about 0.527.

The reasons for this are twofold: (a) the data at 15.598 K are discontinuous around the interface between liquid and solid. Since on the inside of the cell, H_2–D_2 solidified faster than on the outside, the interface was not horizontal, as shown in figure 9. As the incident line laser passed through the interface, the path of laser was changed (refraction, reflection, or scattering), and this part of the laser did not project on the screen. That led to a partial data loss of solid H_2–D_2. The H_2 molar fraction of solid was small, and thus the loss of solid data resulted in a large H_2 molar fraction of the overall H_2–D_2.

(b) On the inner surface of the copper cell, H_2–D_2 solidified faster, so there was more solid H_2–D_2 on both sides than in the middle (measurement position), as shown in figure 9. Similarly, since the content of D_2 in the solid was higher, the H_2 molar fraction of liquid H_2–D_2 increased at the measurement location.

This issue does reflect a limitation of our experiment, but it does not prevent us from observing inhomogeneity in the solid H_2–D_2.

The mole fraction vertical distribution of H_2 at various temperatures is summarized in figure 10. The mole fraction of H_2 in liquid phase was relatively uniform. On the other hand, in solid phase at the lower side of the cell, H_2 has a wider mole fraction. The composition of solid H_2–D_2 was inhomogeneous. The range of the mole fraction of H_2 was found to be from about 0.35–0.60. It is mentioned that the mole fraction of H_2 in solid increased approaching the interface between solid

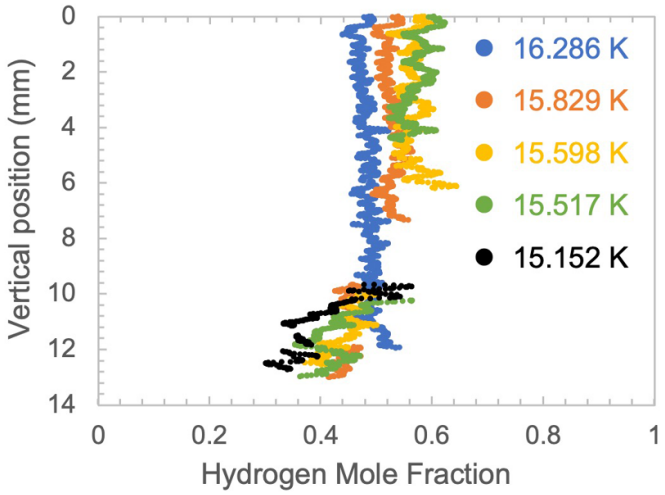

Figure 10. Vertical distribution of mole fraction of H_2. The original H_2–D_2 composition was about 48:52. (Five typical data are shown in this chart for clarity.)

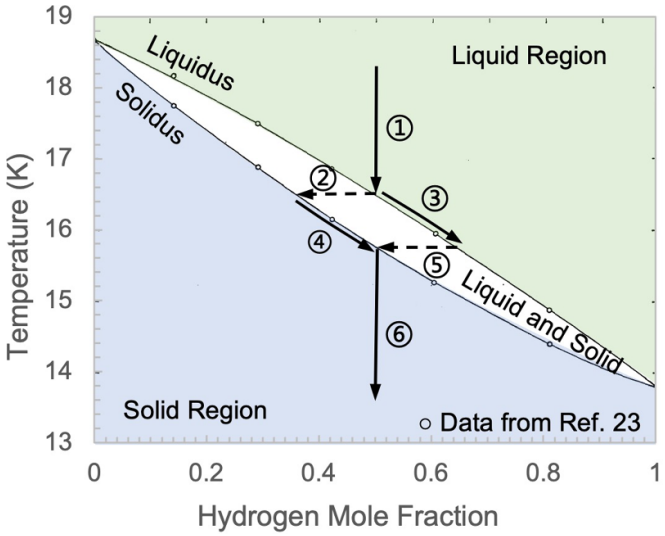

Figure 11. Phase diagram of hydrogen–deuterium. The solid strokes represent the actual change in H_2 mole fraction. The dashed strokes represent the instantaneous change in H_2 mole fraction.

and liquid. The primary crystal that has higher D_2 content was formed at the bottom of the cell.

The phase diagram of H_2–D_2 at cryogenic temperature is shown in figure 11 [23]. Solid H_2–D_2 mixture is a completely soluble solid solution (H_2 and D_2 are soluble at all concentrations). In an equilibrium condition, the mole fraction of H_2 in the H_2–D_2 solid becomes a constant and the solid is a single phase. The phase change in the equilibrium condition is described as follows. The numbers in figure 11 indicate the solidification process.

(1) As an example, a 50/50 H_2–D_2 mixture is used. The mixture is cooled down to the liquidus line. The mixture is a single liquid phase. During the solidification process of liquid H_2–D_2, the liquid and solid phases appear .
(2) The H_2–D_2 solid (primary crystal) appears when the temperature of H_2–D_2 drops below the liquidus line. Since D_2 has a higher freezing point than H_2, D_2 solidifies (crystallizes) faster. The H_2–D_2 solid (primary crystal) is more enriched in the D_2 component. In this case, the primary crystal is formed at 16.600 K and its composition is 0.36 of mole fraction of H_2. This composition means that the D_2 content of solid H_2–D_2 is higher than that of the original composition.
(3) Crystal formation continues, and the composition of H_2 in the liquid phase increases with decreasing temperature because D_2 is extracted into the solid phase. The composition of liquid will change along the liquidus line.
(4) Meanwhile, the crystals exchange material with the H_2-rich solution. The composition of the solid H_2 is moving down the solidus line. Finally, the composition of D_2 in the solid is recovered into the original composition.
(5) When the solidification is complete, the residual liquid is completely solidified, and the liquid phase disappears.
(6) The H_2 mole fraction in solid phase (terminal crystal) becomes a constant at different temperatures.

The temperature and refractive index of each measurement point was obtained, and the relationship between refractive index and temperature is shown in figure 12. We can observe the change in the H mole fraction during solidification.

(1) The H_2–D_2 mixture was cooled down. The ratio of H_2 and D_2 was about 48:52.
(2) The primary crystal of H_2–D_2 appeared at 16.100 K. The liquid H_2–D_2 reached supercooling state.
(3) The composition of liquid H_2–D_2 changed along the direction of the liquidus line.
(4) As solidification continued, the composition of solid H_2–D_2 did not change along the solidus line. This could be explained by the fact that the D_2-rich crystals continually precipitated at the bottom of the cell, and the later-formed crystals covered the previous ones (see figure 3) and prevented the material exchange between the previously formed crystals and solution.
(5) On the other hand, as the composition of H_2 in the liquid phase increased with continuing removal of crystals, the successively formed crystals became continuously more H_2; thus, the terminal crystal had higher H_2 content. The diffusion of H_2 and D_2 in solid phase was too slow to form a homogeneous solid within the measurement period (around 3 h). Finally, each crystal in the solid had a different composition.

Each point on this chart (figure 12) is the H_2 mole fraction at a different temperature. Because the scale of this chart is too large, it looks like a straight line.

Very few studies about solid D_2–T_2 mixture have been reported. In McKenty *et al* [24], the distribution of D_2–T_2 in a solid is simulated with H_2–D_2 data experimentally obtained. The distribution of H_2–D_2 is obtained by the IR transmission coefficient of H_2–D_2 data. The experimental results show a 10.5% variation in deuterium fraction across the cryogenically

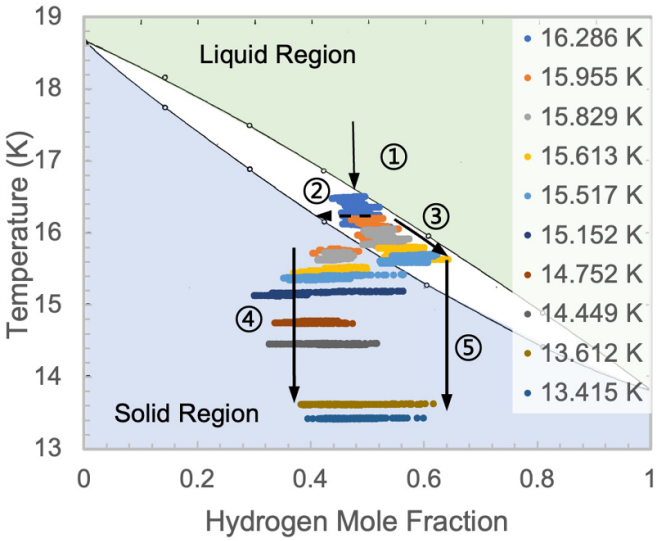

Figure 12. Solidification of H_2–D_2 molecule in this study in view of the change in refractivity index measurement.

formed layer of the solid H_2–D_2 sample. In our experiment, the range of the H_2 mole fraction was from 0.396 to 0.599 in solid H_2–D_2 (terminal crystal). The variation in deuterium fraction is about 20%. McKenty *et al* [24] also supported our observation that the inhomogeneity of the mole fraction in solid appeared during the solidification. However, the variation in deuterium fraction is larger than the literature data. There are two possible reasons: (a) the solidification process proceeded so fast that the later-formed crystals quickly covered the previously formed crystals, preventing the material exchange between the previously formed crystals and the solution. (b) The experiment time was insufficient. The content of D_2 in the solid phase did not reach an equilibrium state during the measurement period. In figure 12, the range of the H_2 mole fraction was 0.384–0.617 at 13.612 K; the range of the H_2 mole fraction was 0.396–0.599 at 13.612 K. The range narrowed; if it took more time, the scope might be narrowed down a bit more.

On the other hand, the decay heat of T would help the D_2–T_2 re-arrangement to be homogeneous in the solid. However, we have no result for the D_2–T_2 rearrangement in ice. This point is an important matter for D_2–T_2 solid in fusion fuel production. Because of isotopic exchange, D_2–T_2 takes place among D_2, Deuterium Tritide (DT), and T_2. The tritium decay heat can accelerate the rate of exchange reaction [25]. The half-time for this reaction has been estimated to be about 18 h in the 21 K liquid D_2–T_2 [26]. The Lorentz–Lorenz mixing rule is also applicable to the calculation of refractive index in ternary mixture [27]

$$\frac{{n_{\mathrm{D-T}}}^2-1}{{n_{\mathrm{D-T}}}^2+2}=\sum_{i=\mathrm{D,\,DT,\,T}}\left(\frac{n_i^2-1}{n_i^2+2}\right)\cdot\phi_i. \tag{15}$$

For the analysis of the D_2–T_2 phase diagram, a ternary phase diagram will be used [25]. In addition, tritium decays to helium-3, which has a boiling point of 4.2 K. Gaseous ^{3}He will escape from the liquid or solid D_2–T_2 and will not affect the refractive index of D_2–T_2.

4. Conclusion

This study demonstrated a method for the high-precision characterization of homogeneity using optical measurements of the refractive index distribution of solid hydrogen isotopologue. This technique has been demonstrated for liquid and solid H_2–D_2 mixture for observing the hydrogenic isotopologue fractionation without the effects of beta decay. Before characterizing the solid D_2–T_2 properties, as a quasi-experiment, we used a H_2–D_2 mixture in which the 1:1 ratio of H and D, mimicked the D_2–T_2 mixture situation. The homogeneity of solid H_2–D_2 was measured.

The experiment results showed that H and D were spatially inhomogeneous to H_2–D_2 during the solidification process. This can be explained by the H_2–D_2 phase diagram and the molecular mobility in solid phase. Since D_2 has a higher freezing point, D_2 solidified from the solution faster than H, and the D-rich solid H_2–D_2 precipitated at the bottom of the cell. As crystallization continued, H-rich crystals were produced. But diffusion was slow in the solid H_2–D_2, causing D-rich crystals and H-rich crystals to exist at the same time. Therefore, the spatial inhomogeneity of D_2–T_2 can be anticipated during D–T fuel solidification. This is a step towards the characterization of D–T, but this will be complicated due to the presence of DT. At present, we have no experimental results of solid D_2–T_2 homogeneity. This work is significant for the fabrication of D–T fuel pellet.

The experiments prove that the method of characterization of solid H_2–D_2 using refractive index distribution is effective, and the same method can characterize solid D_2–T_2. This characterization method has the potential to be practical and usable in the characterization of solid D–T fuel pellets for fusion reactors in the future. The study of D_2–T_2 properties will encourage the production of higher-quality D–T fuel pellets.

Acknowledgments

This work was supported by JSPS KAKENHI Grant Number 22H01204. the Collaboration Research Program between the National Institute for Fusion Science and the Institute of Laser Engineering at Osaka University, and the Hydrogen Isotope Research Centre, Toyama University.

ORCID iDs

Jiaqi Zhang https://orcid.org/0000-0001-5603-1592
Keisuke Shigemori https://orcid.org/0000-0002-3978-8427
Kohei Yamanoi https://orcid.org/0000-0003-4492-4099

References

[1] Murray R.L. and Holbert K.E. 2020 *Nuclear Energy: An Introduction to the Concepts, Systems, and Applications of Nuclear Processes* vol 26, 8th edn (Waltham, MA: Elsevier Inc.) p 526

[2] Hofer J.K. and Foreman L.R. 1988 Radioactively induced sublimation in solid tritium *Phys. Rev. Lett.* **60** 1310–4

[3] Bittner D.N., Collins G.W., Monsler E. and Letts S. 1999 Forming uniform HD layers in shells using infrared radiation *Fusion Sci. Technol.* **35** 244–9

[4] Harding D.R., Wittman M.D. and Edgell D.H. 2012 Considerations and requirements for providing cryogenic targets for direct-drive inertial fusion implosions at the national ignition facility *Fusion Sci. Technol.* **63** 95–105

[5] Iwano K., Iwamoto A., Yamanoi K., Arikawa Y., Nagatomo H., Nakai M. and Norimatsu T. 2021 Preliminary cryogenic layering by the infrared heating method modified with cone temperature control for the polystyrene shell FIREX target *Plasma Fusion Res.* **16** 1404099

[6] Iwamoto A., Fujimura T. and Norimatsu T. 2020 Void free fuel solidification in a foam shell FIREX target *Plasma Fusion Res.* **15** 2404006

[7] Combs S.K. and Baylor L.R. 2018 Pellet-injector technology—brief history and key developments in the last 25 years *Fusion Sci. Technol.* **73** 493–518

[8] Iwano K., Zhang J., Iwamoto A., Iwasa Y., Shigemori K., Hara M., Hatano Y., Norimatsu T. and Yamanoi K. 2022 Refractive index measurements of solid deuterium-tritium *Sci. Rep.* **12** 2223

[9] Childs G.E. and Diller D.E. 1995 Refractive index of liquid deuterium *Adv. Cryst. Energy* **15** 65

[10] Goodwin R.D., Diller D.E., Roder H.M. and Weber L.A. 1961 The densities of saturated liquid hydrogen *Cryogenics* **2** 81

[11] Roder H.M. 1977 *The thermodynamic properties of slush hydrogen and oxygen* (Gaithersburg, MD: National Institute of Standards and Technology) pp 77–859

[12] Kerr E.C. 1952 Molar volumes of liquid deuterium and of a 1: 1 mixture of tritium and deuterium, 19.5–24.5 K *J. Am. Chem. Soc.* **74** 824

[13] Roder H.M., Childs G.E., McCarty R.D. and Angerhofer P.E. 1973 *Survey of the Properties of the Hydrogen Isotopes below Their Critical Temperatures* vol 641 (Gaithersburg, MD: National Bureau of Standards Technology) p 14

[14] Narendra K., Narayanamurthy P. and Srinivasu C. 2011 Refractive indices of binary liquid mixture at different temperatures *Asian J. Appl. Sci.* **4** 535

[15] Diller D.E. 1968 Refractive index of gaseous and liquid hydrogen *J. Chem. Phys.* **49** 3096

[16] McCarty R.D., Hord J. and Roder H.M. 1981 *Selected Properties of Hydrogen (Engineering Design Data) NBS Monograph* vol 168 (Washington, DC: National Bureau of Standards) pp 4–6

[17] Hoge H.J. and Arnold R.D. 1951 Vapor pressures of hydrogen, deuterium, and hydrogen deuteride and dew-point pressures of their mixtures *J. Res. Natl Bur. Stand.* **47** 63–74

[18] Silvera I.F. 1980 The solid molecular hydrogens in the condensed phase: fundamentals and static properties *Rev. Mod. Phys.* **52** 416

[19] Sandler Y.L. 1952 The ortho-para conversion of deuterium in molecular electric fields *J. Chem. Phys.* **20** 1050

[20] Iwamoto A., Fujimura T., Nakai M., Norimatsu T., Sakagami H., Shiraga H. and Azechi H. 2013 FIREX foam cryogenic target development: residual void reduction and estimation with solid hydrogen refractive index measurements *Nucl. Fusion* **53** 4

[21] Niemes S., Telle H.H., Bornschein B., Fasselt L., Größle R., Priester F., Schlösser M., Sturm M., Welte S. and Zeller G. 2021 Accurate reference gas mixtures containing tritiated molecules: their production and Raman-based analysis *Sensors* **21** 6170

[22] Woolley H.W., Scott R.B. and Brickwedde F.G. 1948 Compilation of thermal properties of hydrogen in its various isotopic and ortho-para modifications *J. Res. Natl Bur. Stand.* **41** 395

[23] White D. and Grenier J.R. 1965 Liquid-solid phase equilibria in the hydrogen-deuterium system *J. Chem. Phys.* **42** 4152

[24] McKenty P.W., Wittman M.D. and Harding D.R. 2006 Effect of experimentally observed hydrogenic fractionation on inertial confinement fusion ignition target performance *J. Appl. Phys.* **100** 073302

[25] Lda T., Okuno K. and Naruse Y. 1992 Hydrogen isotope exchange reaction rates in tritium, hydrogen, and deuterium mixed gases *Radiochim. Acta* **56** 209

[26] Souers P.C., Fearon D., Garza R., Kelly E.M., Roberts P.E., Sanborn R.H., Tsugawa R.T., Hunt J.L. and Poll J.D. 1979 Infrared spectra of liquid and solid DT and T_2 *J. Chem. Phys.* **70** 1583

[27] Sechenyh V.V., Legros J.C. and Shevtsova V. 2011 Experimental and predicted refractive index properties in ternary mixtures of associated liquids *J. Chem. Thermodyn.* **43** 1705